Soft Matter

ROYAL SOCIETY OF CHEMISTRY

PAPER

View Article Online
View Journal | View Issue

Cite this: *Soft Matter*, 2021, **17**, 5319

Bulging and budding of lipid droplets from symmetric and asymmetric membranes: competition between membrane elastic energy and interfacial energy†

Meng Wang and Xin Yi *

Lipid droplets are ubiquitous intracellular organelles regulating the storage and hydrolysis of neutral lipids, and play key roles in cellular metabolism and other functions such as protein trafficking and coordinating with immune responses. Though lipid droplets are widely observed in eukaryotic organisms, it remains unclear how and what aspects of mechanical interaction between the neutral lipids and lipid membranes contribute to the bulging and budding of nascent lipid droplets from the endoplasmic reticulum, and particularly effects of membrane asymmetry and spontaneous curvature on lipid droplet formation are not theoretically rationalized. Here we conduct a comprehensive theoretical study on the mechanical behaviors of lipid droplets embedded in between two lipid monolayers of the same or different mechanical properties, and indicate that the membrane bending rigidity, tension and spontaneous curvature, lipid droplet size, and interfacial energy between the neutral lipids and covering lipid leaflets collectively play key roles in regulating the growth and budding transition of lipid droplets. It is found that the embedded neutral lipids beyond a critical volume could undergo a discontinuous shape transition from a lens-like configuration to a budding state with a spherical bulge configuration. Moreover, a positive lipid monolayer spontaneous curvature and smaller monolayer bending rigidity and tension facilitate the budding transition. Budding phase diagrams accounting for these characteristic interaction states are established. Based on the membrane theory at small deformation before budding and the assumption of spherical configuration after budding, we obtain analytical solutions on the bulge profiles, which can be used to estimate the value of interfacial energy. Our results uncover the fundamental mechanics of the lipid droplet formation and budding, and are of broad interest to the studies of echogenic liposome stability and cellular incorporation of nanoparticles.

Received 16th February 2021,
Accepted 12th April 2021

DOI: 10.1039/d1sm00245g

rsc.li/soft-matter-journal

1 Introduction

Lipid droplets, consisting of hydrophobic neutral lipid cores enclosed by phospholipid monolayers decorated by specific proteins, are ubiquitous metabolic organelles in most cell types, and play important roles in lipid metabolism, membrane synthesis, and energy homeostasis.[1–4] During the biogenesis of lipid droplets, neutral lipids, synthesized between leaflets of the endoplasmic reticulum (ER) membrane, accumulate and form an oil lens with increasing lipid concentration in a process of demixing. As the lipid core progressively grows, the lipid droplet undergoes a shape transformation from a lens-like shape to a nearly spherical bulge, which could detach from the ER membrane and stay in the cytosol before degeneration due to the lipid remobilization.[1–3,5] Over the past decade, interest in the specific biological pathways coordinating the biogenesis of lipid droplets has been increasing, and there exist extensive studies on the existence and underlying mechanisms of lipid droplet diversification in regard to the specific protein or lipid compositions, and significant progress toward understanding where and how lipid droplets are formed and coordinated from the viewpoint of cell biology.[1–3,5,6]

In contrast, much less studies (mainly experiments) have been devoted to the mechanical and biophysical behaviors of lipid droplets such as budding size, lipid droplet asymmetry and directional budding. For example, the monolayer tension asymmetry regulates the droplet budding side.[7,8] Fat storage-inducing transmembrane (FIT) proteins could promote lipid droplet budding,[9] and asymmetric insertion of membrane

Department of Mechanics and Engineering Science, College of Engineering, Peking University, Beijing 100871, China. E-mail: xyi@pku.edu.cn

† Electronic supplementary information (ESI) available: Profiles of lipid droplets and system energy evolution at finite spontaneous curvature or with monolayer tension asymmetry are provided. Comparison between present and previous case studies for two identical monolayers at zero spontaneous curvature is also provided. See DOI: 10.1039/d1sm00245g

proteins regulates the emergence side of model lipid droplets.[8] Further experimental studies indicate that FIT protein 2 can also regulate the lipid droplet emergence by reducing the level of ER diacylglycerol, a type of lipids with negative spontaneous curvature.[10] It is reported that the budding size of lipid droplets is affected by membrane composition and for phospholipids exhibiting relatively low tension a small droplet size is observed.[11] More recently molecular dynamics simulations have been employed to investigate the early stage of lipid droplet formation with focus on the structural roles of lipid molecules on lipid droplet growth.[12,13]

Despite experimental studies and molecular simulations on these biophysical processes, so far there have been only few theoretical studies dedicated to the bulging and budding of lipid droplets from a mechanical viewpoint.[14,15] For example, the lipid droplet has been simply modelled as a spherical cap on a flat lipid monolayer during budding, leading to an oversimplified system configuration evolution.[14] In a recent theoretical study, the lipid droplet formation in a symmetric lipid membrane with zero spontaneous curvature has been investigated by adopting the Helfrich membrane theory.[15] It is found that the lipid droplet beyond a critical volume undergoes an abrupt morphological transit from a flat lens-like shape of mirror symmetry to an almost spherical protrusion.[15] Analytical results on the profile of the lipid droplet at small membrane deformation are obtained but restricted to the small droplet limit.[15] As the effects of the membrane asymmetry and monolayer spontaneous curvature on the lipid droplet formation have not been taken into account in that work,[15] the budding with directional bias observed in experiments[7,8,10] cannot be predicted.

Nowadays open questions remain on the general mechanical behaviors of lipid droplets such as nonlinear deformation of the lipid monolayers, discontinuous shape transformation of the lipid droplet, and a robust modeling fully and accurately accounting for the effects of membrane mechanical properties particularly spontaneous curvature and their difference or asymmetry on the lipid droplet formation and directional budding is lacked.

In this theoretical work, we systematically investigate the bulging and budding of lipid droplets in symmetric and asymmetric lipid membranes by building a thorough mechanical model incorporating the roles of membrane rigidity, tension and spontaneous curvature, lipid droplet size, and neutral lipid–lipid leaflet interfacial energy. It is revealed that the competition between membrane elastic energy and repulsive interfacial interaction governs the configuration evolution and budding transition of the lipid droplets. A positive lipid monolayer spontaneous curvature and small monolayer bending rigidity and tension could facilitate the budding. Moreover, the effects of monolayer bending rigidity and tension asymmetry of different leaflets on the budding direction are analyzed. Budding phase diagrams demarcating stable embedded states and budding states are established. Analytical predictions on the configurations of lipid droplets of both small and relatively large sizes at initial bulging are provided. Our results offer mechanistic insights on the underlying physics of lipid droplet formation and are of guiding significance for studies of echogenic liposome stability and cell interaction with inserted nanoparticles.

2 Theoretical modeling

A continuum model based on the Helfrich membrane theory is employed here to probe how a lipid bilayer membrane interacts with an embedded lipid droplet of a given volume. As illustrated in Fig. 1, the system is assumed to adopt an axisymmetric configuration with three portions: the inner top (red, #1) and

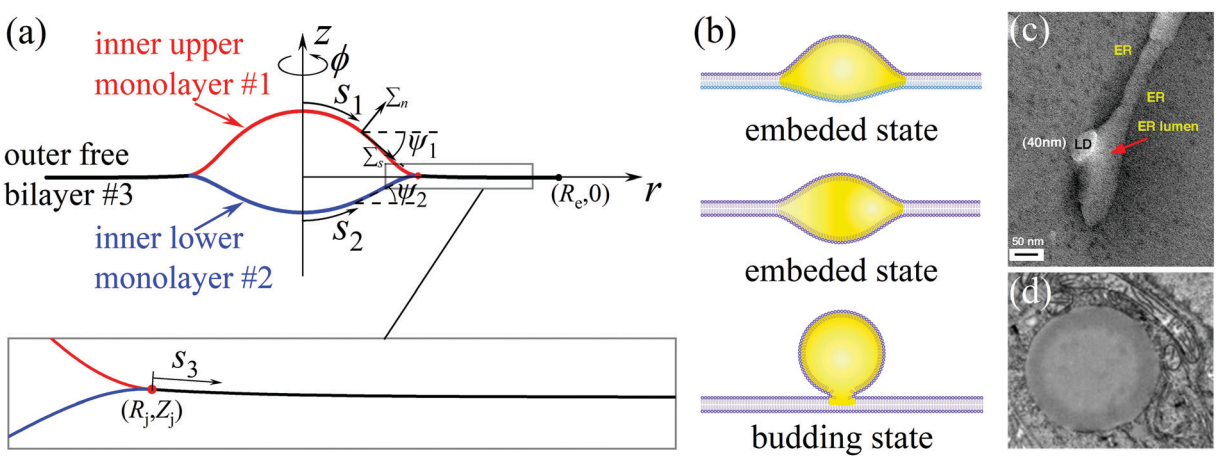

Fig. 1 Axisymmetric configuration of a lipid droplet embedded in a lipid bilayer membrane in a cylindrical coordinate (r, ϕ, z). (a) The system is divided into three portions: the inner upper (red) and lower (blue) lipid monolayers in contact with the embedded lipid droplet, and the outer free bilayer region (black). The geometry of each portion could be characterized by the tangent angle ψ as a function of the arclength s. The tangent angle is positive as measured counterclockwise from the horizontal dashed line. Here ψ_2 is positive and ψ_1 is negative as illustrated. At the junction, the tangent angle, r- and z-coordinates are denoted as ψ_j, R_j, and Z_j, respectively. (b) Schematic configurations for embedded states with or without vertical symmetry and the budding state. Neutral lipid cores (yellow) are confined between two lipid monolayers. (c) Experimental images of a nascent lipid droplet (LD) confined in an ER membrane. Reprinted with permission from ref. 9. Copyright 2015 Choudhary *et al.* Originally published in *Journal of Cell Biology*. (d) High magnification electron micrograph of a lipid droplet in a rat hepatoma cell. Reprinted from ref. 17. Copyright 2009, with permission from Elsevier.

bottom (blue, #2) lipid monolayers in contact with the embedded lipid droplet, and the outer free bilayer region (black, #3). Quantities pertaining to these three regions are identified by subscripts 1, 2, and 3, respectively, unless otherwise stated. The total energy E_{tot} of the system in the cylindrical coordinate (r, ϕ, z) is described as

$$\begin{aligned} E_{\mathrm{tot}} &= E_{\mathrm{bend}} + E_{\mathrm{ten}} + E_{\mathrm{intf}}, \\ E_{\mathrm{bend}} &= \sum_{i=1,2} \frac{\kappa_i}{2} \int \left(2M_i - c_i^{(0)}\right)^2 \mathrm{d}A_i \\ &\quad + \int \sum_{i=1,2} \frac{\kappa_i}{2} \left(\pm 2M_3 - c_i^{(0)}\right)^2 \mathrm{d}A_3, \\ E_{\mathrm{ten}} &= \sum_{i=1,2,3} \sigma_i \Delta A_i, \quad \text{and } E_{\mathrm{intf}} = \sum_{i=1,2} \gamma_i A_i, \end{aligned} \tag{1}$$

where E_{bend} is the elastic bending energy of the membrane as a Canham–Helfrich functional[16] with κ_i, M_i, $c_i^{(0)}$ and $\mathrm{d}A_i$ representing the bending rigidity, mean curvature, spontaneous curvature and surface element of the membrane, respectively (i = 1, 2, 3). Here we assume that two monolayers in the outer free region stay in perfect contact and form a bilayer membrane with a bending rigidity of $\kappa_1 + \kappa_2$. In the second term of E_{bend}, the positive and negative signs before $2M_3$ are associated with the top and bottom leaflets, respectively. E_{ten} describes the membrane tension energy with σ_i as the membrane tension conjugated to the excess area ΔA_i induced by the lipid droplet (i = 1, 2, 3). Here we have $\sigma_3 = \sigma_1 + \sigma_2$ in the outer free region. γ_i, contributing the interfacial energy E_{intf}, represents the effective interfacial energy per unit area of contact owing to the nonpolar interaction between the neutral lipid core and lipid tail groups of the monolayers (i = 1, 2) with a ground energy cost of the nonpolar interaction between facing lipid tail groups in a pure lipid bilayer. As the latter nonpolar interaction is stronger than the former one, the interfacial energy is repulsive with a positive γ_i. Such effective repulsive interaction results in the self-assembly or accumulation of neutral lipids in the ER membrane to reduce the nonpolar interaction energy cost. To simplify the following analysis, we further assume $\gamma_1 = \gamma_2 = \gamma$ and $c_1^{(0)} = c_2^{(0)} = c_0$.

From a mechanical viewpoint, one can see that the embedded lipid droplet of a flat lens-like shape is favored by the membrane elastic energy $E_{\mathrm{bend}} + E_{\mathrm{ten}}$ to save the energetic cost of membrane bending and tension, while the interfacial energy E_{intf} prefers outward spherical bud-off as a sphere has the smallest surface area for a given enclosed volume. The competition between membrane elastic energy and interfacial energy regulates the bulging and budding of lipid droplets as analyzed in the following sections.

In the axisymmetric configuration, the mean curvature is $M_i = (\mathrm{d}\psi_i/\mathrm{d}s_i + \sin\psi_i/r_i)/2$ and the excess surface area is $\Delta A_i = 2\pi\int_0^{l_i} r_i(1-\cos\psi_i)\mathrm{d}s_i$ with l_i as the unknown total arclength of each region (i = 1, 2, 3). The area of each inner monolayer is $A_i = 2\pi\int_0^{l_i} r_i \mathrm{d}s_i$ (i = 1, 2), and the lipid droplet volume is $V = \pi\int_0^{l_2} r_2^2 \sin\psi_2 \mathrm{d}s_2 - \pi\int_0^{l_1} r_1^2 \sin\psi_1 \mathrm{d}s_1$. Here we have used the geometric relations $\mathrm{d}r_i/\mathrm{d}s_i = \cos\psi_i$ and $\mathrm{d}z_i/\mathrm{d}s_i = \sin\psi_i$. Introducing $t_i = s_i/l_i (\in [0, 1])$ for each membrane portion, the elastic energy of the system can be expressed in terms of the unknown functions $\psi_i(t_i)$, which can then be approximated by cubic B-spline curves as $\psi_i(t_i) = \sum_{j=1}^{n} a_j^{(i)} N_j^{(i)}(t_i)$, where the basis functions $N_j^{(i)}(t_i)$ are defined recursively on a non-uniform knot vector of t_i. A typical choice of the knot vector of t_i is $\{t_i^{(0)}, t_i^{(1)}, t_i^{(2)}, \ldots, t_i^{(n+4)}\}$ with $t_i^{(k)} = 0$ (k = 0, 1, 2, 3) and $t_i^{(k)} = 1$ ($k = n+1, \ldots, n+4$). The expression of the cubic B-spline basis functions $N_j^{(i)}(t_i)$ can be found in the appendix of ref. 18.

Numerical optimization method is used to determine the minimum energy state of the system at a given volume of the lipid droplet. Several boundary conditions are imposed. The axisymmetric and smooth configuration requires $\psi_1(0) = \psi_2(0) = 0$ at $r_1 = r_2 = 0$. At the junction between inner monolayers and the outer free bilayer ($t_1 = t_2 = 1$ or $t_3 = 0$), the continuity of ψ, r and z are required. At the remote boundary ($r_3 = R_{\mathrm{e}}$), we have $z_3 = 0$, meanwhile $\psi_3 = 0$ is imposed to enforce the flatness of the bilayer far away from the embedded lipid droplet. Here $R_{\mathrm{e}} = 10a$ is taken. The lipid droplet volume V is enforced by introducing an equality constraint. At a given V, the minimum system energy is obtained via the interior point optimization approach after deriving the first and second derivatives of E_{tot} in eqn (1) and the volume constraint with respect to parameters $a_j^{(i)}$ and l_i. In our calculations, all lengths are rescaled by the effective radius of the lipid droplet $a = [3V/(4\pi)]^{1/3}$. The system energy then becomes $E_{\mathrm{tot}} = E_{\mathrm{tot}}(\bar{\sigma}_1, \bar{\sigma}_2, \bar{\gamma}, c_0 a, \kappa_2/\kappa_1)$ with the dimensionless parameters defined as

$$\bar{\sigma}_i = 2\sigma_i a^2/\kappa_1 \ (i = 1, 2) \quad \text{and } \bar{\gamma} = 2\gamma a^2/\kappa_1.$$

3 Results and discussion

3.1 Lipid droplet in two chemically identical monolayers

Before we systematically investigate the lipid droplet morphology in a general case, we consider a simple condition that the lipid membrane is composed of two chemically identical monolayers of spontaneous curvature c_0, bending rigidity $\kappa (= \kappa_1 = \kappa_2)$, and tension $\sigma (= \sigma_1 = \sigma_2)$. In this case, the bilayer portion is flat and has zero mean curvature.

In this subsection, we first seek analytical prediction on the initial local bulging of the lipid droplet based on small membrane deformation and then perform fully nonlinear analysis on the mechanical behaviors of the system undergoing budding transition.

3.1.1 Analytical solutions for the initial bulging of a lipid droplet. At relatively large membrane tension or small repulsive interfacial energy, the lipid droplet before budding adopts a flat lens-like shape, and the system configuration can be approximated by a perturbation from a flat conformation as follows. Due to the vertical symmetry of the system, the outer free bilayer is flat and our theoretical analysis is focused on the inner contact region. For simplicity, the subscripts associated with quantities pertaining to the contact region are ignored.

In the cylindrical coordinate (Fig. 1a), the local membrane force per unit circumferential length can be expressed as[19]

$$\begin{aligned}\Sigma_s &= \frac{\kappa}{2}c_0(c_0-2c_2)+\sigma+\gamma+\frac{\kappa}{2}(c_2^2-c_1^2),\\ \Sigma_n &= -\kappa\frac{\mathrm{d}(c_1+c_2)}{\mathrm{d}s},\end{aligned} \tag{2}$$

where Σ_n and Σ_s represent the out-of-plane shear force along the inward normal direction and in-plane force along the meridional direction, respectively, and the principal curvatures in the meridional and circumferential directions are denoted by $c_1 = \mathrm{d}\psi/\mathrm{d}s$ and $c_2 = \sin\psi/r$, respectively.

For the inner upper monolayer, a force balance along the z-axis leads to the governing equation

$$2\pi r(\Sigma_s\sin\psi + \Sigma_n\cos\psi) = -p\pi r^2, \tag{3}$$

where p, originating from the volume constraint of the lipid droplet, represents an effective pressure difference between the lipid droplet and external environment.

At small deformation ($|\mathrm{d}z/\mathrm{d}r| \ll 1$), we have

$$\sin\psi \approx \frac{\mathrm{d}z}{\mathrm{d}r},\quad \cos\psi\approx 1,\quad \frac{\mathrm{d}\psi}{\mathrm{d}s}\approx\frac{\mathrm{d}^2z}{\mathrm{d}r^2},\quad \frac{\mathrm{d}^2\psi}{\mathrm{d}s^2}\approx\frac{\mathrm{d}^3z}{\mathrm{d}r^3}. \tag{4}$$

Substituting eqn (4) into eqn (2) and retaining the leading orders in z and its derivatives with respect to r, eqn (2) reduces to

$$\begin{aligned}\Sigma_s &= \frac{1}{2}\kappa c_0^2-\kappa c_0\frac{1}{r}\frac{\mathrm{d}z}{\mathrm{d}r}+\sigma+\gamma,\\ \Sigma_n &= -\kappa\left(\frac{\mathrm{d}^3z}{\mathrm{d}r^3}+\frac{1}{r}\frac{\mathrm{d}^2z}{\mathrm{d}r^2}-\frac{1}{r^2}\frac{\mathrm{d}z}{\mathrm{d}r}\right).\end{aligned} \tag{5}$$

With the help of eqn (4) and (5), the governing equation for the monolayer shape $z = z(r)$ in a form of a linear modified Bessel differential equation can be obtained from eqn (3) as

$$r^2\frac{\mathrm{d}^3z}{\mathrm{d}r^3}+r\frac{\mathrm{d}^2z}{\mathrm{d}r^2}-\left[1+\left(\frac{\sigma+\gamma}{\kappa}+\frac{c_0^2}{2}\right)r^2\right]\frac{\mathrm{d}z}{\mathrm{d}r}=\frac{p}{2\kappa}r^3, \tag{6}$$

where effects of σ, γ, p, κ, and c_0 on the membrane shape $z = z(r)$ are explicitly considered.

In the case of a localized vertical force f along z-axis instead of a pressure p, the term pr^3 on the right-hand side of eqn (6) should be changed to fr/π.[20]

Note that in literature another governing shape equation of $\psi = \psi(r)$ restricted with $c_0 = 0$ has been obtained at small monolayer deformation based on the variation of the total system energy [eqn (29) in the ESI of ref. 15]. In its derivation, the linear order in ψ has been only retained in terms without association to the tension and ignored in the tension term with the aim of deriving approximate expression in the small lipid droplet limit, leading to a simple equation without the effect of σ and γ. As the membrane tension can suppress bulging, the governing equation in ref. 15 is expected to overestimate the membrane deformation compared with eqn (6) as confirmed in later comparison in this subsection. Compared to ref. 15, eqn (6) in the present work is not restricted to the case of small lipid droplets and can offer more precise analytical prediction in cases of both small and relatively large lipid droplets.

With the boundary condition of $\psi = 0$ at $r = 0$, eqn (6) can be solved as

$$\frac{\mathrm{d}z}{\mathrm{d}r}=\frac{p}{2\beta^2\kappa}\left[-1+\frac{R_\mathrm{j}}{r}\frac{I_1(\beta r)}{I_1(\beta R_\mathrm{j})}\right]r+\frac{I_1(\beta r)}{I_1(\beta R_\mathrm{j})}\tan\psi_\mathrm{j}, \tag{7}$$

where $\beta=\sqrt{(\sigma+\gamma)/\kappa+c_0^2/2}$, R_j and ψ_j denote the unknown r-coordinate and tangent angle at the triple junction between two inner monolayers and the outer bilayer membrane, and I_1 represents the first order of the modified Bessel function of the first kind. Integrating eqn (7) with respect to r gives

$$\begin{aligned}z(r) = z(R_\mathrm{j}) &- \frac{\tan\psi_\mathrm{j}}{\beta I_1(\beta R_\mathrm{j})}\left[I_0(\beta R_\mathrm{j})-I_0(\beta r)\right]\\ &+\frac{p}{4\beta^2\kappa}\left\{R_\mathrm{j}^2-r^2-\frac{2R_\mathrm{j}}{\beta I_1(\beta R_\mathrm{j})}\left[I_0(\beta R_\mathrm{j})-I_0(\beta r)\right]\right\},\end{aligned} \tag{8}$$

where I_0 represents the zeroth order of the modified Bessel function of the first kind.

In the case of two identical monolayers, the system before budding has vertical symmetry, and we have $z(R_\mathrm{j}) = 0$ and $\psi_\mathrm{j} = 0$ at $r = R_\mathrm{j}$, from which eqn (7) and (8) further reduce to

$$\frac{\mathrm{d}z}{\mathrm{d}r}=\frac{p}{2\beta^2\kappa}\left[-1+\frac{R_\mathrm{j}}{r}\frac{I_1(\beta r)}{I_1(\beta R_\mathrm{j})}\right]r \tag{9}$$

and

$$z(r)=\frac{p}{4\beta^2\kappa}\left\{R_\mathrm{j}^2-r^2-\frac{2R_\mathrm{j}}{\beta I_1(\beta R_\mathrm{j})}\left[I_0(\beta R_\mathrm{j})-I_0(\beta r)\right]\right\}, \tag{10}$$

respectively. To obtain the bulge profile $z(r)$, we still need to determine p and R_j in eqn (10). The center height or maximum deflection of the monolayer before budding transition is

$$z_\mathrm{max}=z(r=0)=\frac{pR_\mathrm{j}}{4\beta^2\kappa}\left\{R_\mathrm{j}-\frac{2}{\beta I_1(\beta R_\mathrm{j})}\left[I_0(\beta R_\mathrm{j})-1\right]\right\}.$$

Based on the balance of tangential force[19] at the junction with $\psi_\mathrm{j} = 0$, we have $\gamma = \kappa(\mathrm{d}\psi/\mathrm{d}s)^2/2$ at $r = R_\mathrm{j}$, which at the small membrane deformation is further approximated as

$$\gamma\approx\frac{\kappa}{2}\left(\frac{\mathrm{d}^2z}{\mathrm{d}r^2}\right)^2\quad\text{at } r=R_\mathrm{j}.$$

Then we obtain an approximation of γ at small monolayer deformation as

$$\gamma=\frac{p^2R_\mathrm{j}^2I_2^2(\beta R_\mathrm{j})}{8\kappa\beta^2I_1^2(\beta R_\mathrm{j})}. \tag{11}$$

Though the r-coordinate R_j of the triple junction and the effective pressure p are related via eqn (11), they remain unknown. From the lipid droplet volume $V/2=2\pi\int_0^{R_\mathrm{j}}rz\mathrm{d}r$, we can obtain p from eqn (10) in terms of R_j as

$$p=\frac{16a^3\beta^2\kappa I_1(\beta R_\mathrm{j})}{3R_\mathrm{j}^4I_3(\beta R_\mathrm{j})}, \tag{12}$$

where $a = [3V/(4\pi)]^{1/3}$ is the effective radius of the lipid droplet. Here we have used the relation $xI_3(x) = xI_1(x) - 4I_2(x)$.

Combining eqn (11) and (12), we have

$$\gamma = \frac{32\kappa a^6 \beta^2 I_2^2(\beta R_j)}{9 R_j^6 I_3^2(\beta R_j)}. \quad (13)$$

Recognizing eqn (13) as a Taylor series at $\beta R_j \ll 1$ (the small lipid droplet limit) and taking the linear term, R_j can be approximately obtained as

$$R_j = \frac{2a}{\bar{\gamma}^{1/8}}. \quad (14)$$

The eqn (14) expressed in a different form has been derived in ref. 15. Substituting eqn (12) and (14) into eqn (10) gives a good analytical prediction on the bulge profile at small deformation (see Fig. 2a and Fig. S1a, S2 in the ESI†). Note that the effects of σ and c_0 on R_j are negligible at $\beta R_j \ll 1$ as eqn (14) indicated, which is confirmed by numerical comparison in Fig. 2b and Fig. S1b (ESI†).

For the case of two identical monolayers with zero spontaneous curvature, another analytical prediction on the bulge profile at small deformation has been obtained in ref. 15, and its comparison with our analytical results and fully nonlinear numerical results is shown in Fig. S2 (ESI†). As discussed in the second paragraph following eqn (6) and confirmed in Fig. S2 (ESI†), that analytical prediction derived in ref. 15 overestimates the bulge deformation of the monolayer and is valid in the small lipid droplet limit.

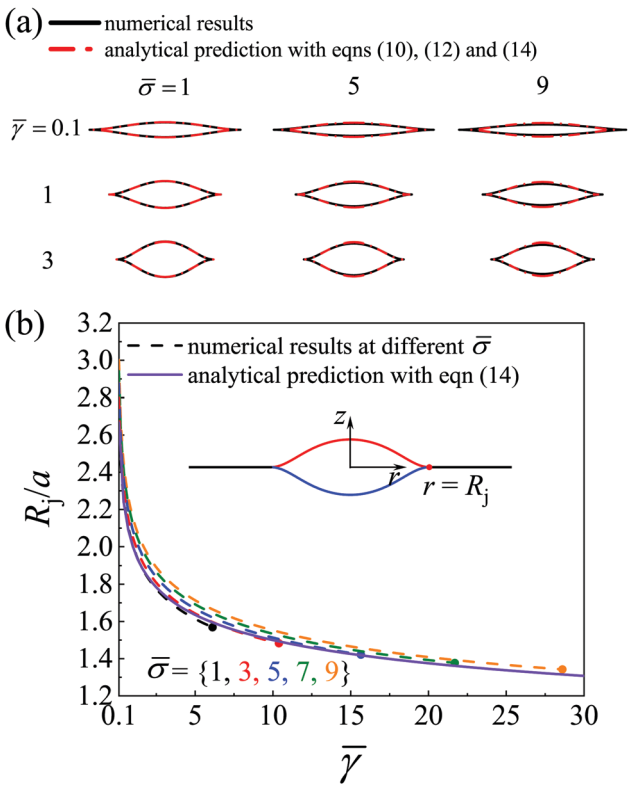

Fig. 2 Comparison between our numerical results using optimization and analytical prediction at zero spontaneous curvature. (a) Selected shapes of the contact region, and (b) r-coordinate R_j of the triple junction.

Substituting R_j in eqn (14) into eqn (12) gives an approximation of p at $\beta R_j \ll 1$ as

$$p = \frac{128a^3\kappa}{R_j^4} = \frac{8\kappa\bar{\gamma}^{1/2}}{a} = 8\sqrt{2\gamma\kappa},$$

which indicates that p is insensitive to σ and c_0, and is proportional to $(\gamma\kappa)^{1/2}$ at $\beta R_j \ll 1$.

In the case of two identical monolayers, the total system energy E_{tot} in eqn (1) is given as

$$E_{tot} = 2\pi\kappa\int_0^l r\left(\frac{d\psi}{ds} + \frac{\sin\psi}{r} - c_0\right)^2 ds + 4(\sigma+\gamma)\pi\int_0^l r ds - 2\sigma\pi R_j^2 + \pi\kappa c_0^2\left(R_e^2 - R_j^2\right), \quad (15)$$

where l is the total arclength of the bulged upper or lower monolayer. At small monolayer deformation, substituting eqn (4) and (9) into eqn (15) gives

$$E_{tot} = \frac{p^2\pi R_j^4(\sigma+\gamma)}{8\beta^4\kappa^2}\left\{3 - \frac{2I_2(\beta R_j)}{I_1(\beta R_j)}\left[\frac{I_0(\beta R_j)}{I_1(\beta R_j)} + \frac{4}{\beta R_j}\right]\right\} + \frac{p^2\pi R_j^2}{4\beta^2\kappa}\left[\frac{R_j^2 I_0^2(\beta R_j)}{I_1^2(\beta R_j)} - R_j^2 - \frac{4}{\beta^2}\right] + \pi\kappa c_0^2 R_e^2 + 2\pi R_j^2\gamma, \quad (16)$$

where p and R_j are given by eqn (12) and (14), respectively. Fig. S2 (ESI†) indicates that the analytical approximation in eqn (16) agrees well with the fully numerical results at small bulge deformation before budding.

3.1.2 Fully nonlinear numerical analysis for the bulging and budding transition. In the above analysis, analytical attention is paid to the initial bulging of the lipid droplet at small membrane deformation. In the case of large membrane deformation, in particular the budding transition, no simple analytical solutions are available and we conduct fully nonlinear analysis on the bulging and budding using numerical optimization. Fig. 3a shows the typical system morphologies at different $\bar{\sigma}$ and $\bar{\gamma}$ with $c_0 = 0$. Two representative stable states are observed. One is the embedded state in which the lipid droplet forms a flat lens-like shape in between two monolayers, and the other one is the budding state in which the lipid droplet forms a nearly spherical bulge on one side of the lipid membrane (upper side in the present work). The transition from the embedded state to the budding state is facilitated by $\bar{\gamma}$ and suppressed by $\bar{\sigma}$ (see Fig. 3a). The lens-like bulge before the budding becomes more flattened as $\bar{\gamma}$ decreases (a lower interfacial energy) or $\bar{\sigma}$ increases (a lower membrane tension energy), since a more flattened configuration gives a larger contact area $A_c = A_1 + A_2$ as well as a smaller excess area $\Delta A_1 + \Delta A_2 = A_c - 2\pi R_j^2$. Once the lipid droplet buds off, the bulge adopts an almost spherical shape with a curved monolayer neck of an infinitesimal toroid radius (see inset in Fig. 3b), and the spherical bulge is about to pinch off from the membrane. To accurately capture the membrane neck, dense meshing in the vicinity of the highly curved region is required (Fig. S3, ESI†). The almost spherical

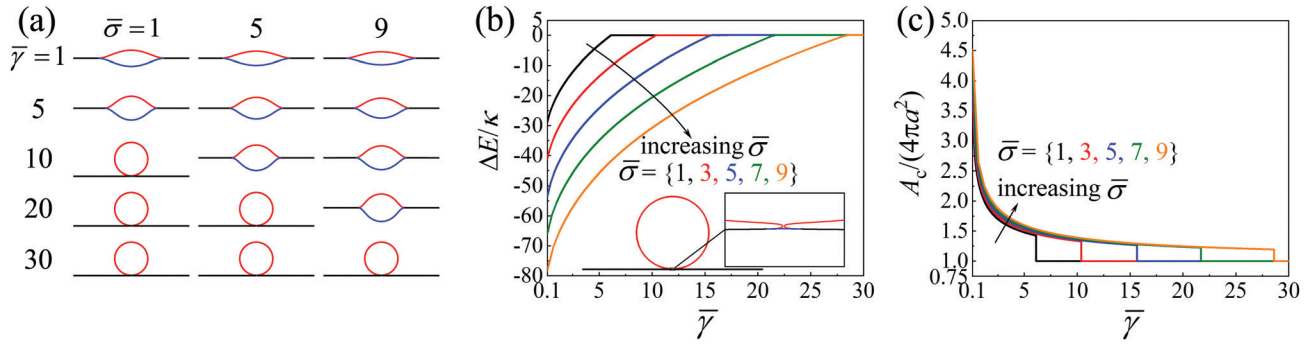

Fig. 3 System configurations, energy gaps, and interfacial contact areas in the case of two identical monolayers of zero spontaneous curvature at different repulsive interfacial energy $\bar{\gamma}$ and membrane tension $\bar{\sigma}$. (a) Selected system configurations at $\bar{\sigma} \equiv 2\sigma a^2/\kappa$ = 1, 5 and 9 and $\bar{\gamma} \equiv 2\gamma a^2/\kappa$ = 1, 5, 10, 20 and 30. (b) Energy gap ΔE as functions of $\bar{\gamma}$ at different $\bar{\sigma}$. (c) Contact area A_c(= A_1 + A_2) versus $\bar{\gamma}$. Inset in (b), illustration of neck in the budding state at $\bar{\sigma}$ = 1, $\bar{\gamma}$ = 10, and c_0 = 0.

bulge leads to $\sum_{i=1,2,3} \sigma_i \Delta A_i + \sum_{i=1,2} \gamma_i A_i \approx 4\pi a^2(\sigma+\gamma) = 2(\bar{\sigma}+\bar{\gamma})\pi\kappa$, which means that the sum of $\bar{\gamma}$ and $\bar{\sigma}$ acts as a joined parameter. As the elastic deformation energy of the narrow neck region is negligible,[21] the total energy E_{tot} in the budding state can be well approximated by

$$E_{tot} = 2\pi\kappa(2 - c_0 a)^2 + 4\pi(\sigma+\gamma)a^2 + \pi\kappa c_0{}^2 R_e{}^2. \quad (17)$$

The accuracy of eqn (17) is confirmed by numerical comparison in Fig. S4 (ESI†).

If the lipid droplet splits into two identical droplets and buds off separately, then we have

$$E_{tot} = 4\pi\kappa(2 - c_0 a/2^{1/3})^2 + 8\pi(\sigma+\gamma)a^2/2^{2/3} + \pi\kappa c_0{}^2 R_e{}^2. \quad (18)$$

In the case of vanishing monolayer spontaneous curvature, E_{tot} in eqn (18) is always larger than E_{tot} in eqn (17), which means that in this case the separate budding is not energetically favorable. Similar phenomena can also be observed in the dispersion of hydrophobic nanoparticles within lipid bilayers[22] and aggregation of adhesive nanoparticles between adjacent lipid membranes.[23]

The shape transformation in Fig. 3a is consistent with the energy analysis in Fig. 3b, in which the curves of the system energy change $\Delta E(\bar{\gamma}) = E_{tot} - E_0$ with E_0 as the ground state energy showing kinks correspond to the discontinuous transition from the embedded state to the budding state. As $\bar{\sigma}$ increases, the value of $\bar{\gamma}$ associated with the kink increases. Here the reference state is taken as a flat bilayer membrane of radius R_e with a spherical monolayer vesicle of radius a (approximating the budding state), and its energy is given by eqn (17) as E_0 = $2\pi\kappa(2 - c_0 a)^2 + 4\pi(\sigma+\gamma)a^2 + \pi\kappa c_0{}^2 R_e{}^2$. Moreover, the slope d($\Delta E$)/d$\bar{\gamma}$ of the energy profile decreases before the shape transition (Fig. 3b), which indicates that the interfacial contact area A_c decreases as $\bar{\gamma}$ increases, consistent with the results in Fig. 3c.

To further elucidate the physical mechanism underlying the budding transition, profiles of the total system energy E_{tot} and its three components E_{bend}, E_{ten}, and E_{intf} are analyzed (Fig. 4). Here we take $\bar{\sigma}$ = 5 as a case study. It is shown that all these three energy components increase nonlinearly as $\bar{\gamma}$ increases for the embedded state, followed by a kink or discontinuous

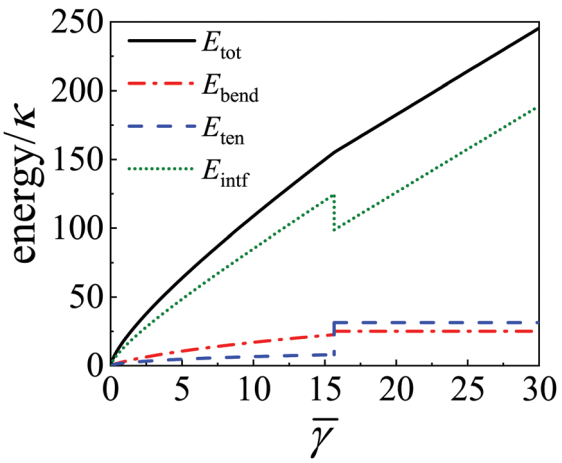

Fig. 4 Total system energy E_{tot} and its three components (the membrane bending energy E_{bend}, membrane tension energy E_{ten}, and interfacial energy E_{intf}) as functions of $\bar{\gamma}$ at c_0 = 0 and $\bar{\sigma}$ = 5.

variations corresponding to the budding transition. The sudden increase experienced by the tension energy E_{ten} is of more extent than that observed in the bending energy E_{bend}, meaning that the energy cost inhibiting the budding transition mainly arises from the monolayer expansion on the budding side at high tension. Upon budding, the system configuration can be approximated by a flat membrane and an almost spherical bulge of radius a. Therefore, in the budding state, the E_{bend} and E_{ten} curves are almost flat and the E_{intf} curve exhibits a linear dependence on $\bar{\gamma}$ as the system configuration does not change. The sudden drop in the E_{intf} curve corresponds to a drop in the contact area A_c as shown in Fig. 3c. As long as the decrease of the repulsive interfacial energy can compensate the increasement of the membrane bending and tension energy, the budding transition occurs. In the cases of vanishing or negative $\bar{\gamma}$, no interfacial tension energy decrease would appear, and hence the lipid droplet would never bud off.

In ref. 15 on the study of the lipid droplet budding from a symmetric membrane, the elastic deformation energy of the inner membranes before budding at $\gamma \gg \sigma$ is further approximated by a phenomenological line energy $E_{line} = 16\pi\sigma_{eff}R_j$ based

on a previous theoretical study on the cell membrane wrapping around a rigid spherical nanoparticle,[24] where σ_{eff} is the effective line tension scaling as $\sqrt{\kappa(\sigma+\gamma)}$ and R_j is the r-coordinate of the lipid layer junction. Though the line energy $E_{\text{line}}(\gamma)$ has the energy unit and σ_{eff} as a parameter provides a phenomenological explanation on the budding transition as $E_{\text{line}}(\gamma)$ displays a trend similar to what eqn (16) exhibits in Fig. S4 (ESI†), $E_{\text{line}}(\gamma)$ in fact overestimates the elastic energy associated with monolayer deformation. More importantly, this phenomenological analysis cannot specify the main or dominant aspect among the membrane bending energy, tension energy and interfacial energy in governing the budding transition, compared with Fig. 4 and relevant discussion in the last paragraph.

Depending on the membrane lipid composition, the geometry of the lipid molecules could vary significantly, and the monolayer spontaneous curvature could have a finite positive or negative value ($c_0 \neq 0$). For example, the lipid monolayers composed of phosphatidylinositol and monoacylglycerol molecules have a positive c_0, while diacylglycerol and phosphatidic acid form lipid monolayers with a negative spontaneous curvature.[1,25] The lipid spontaneous curvature has been demonstrated experimentally to affect the lipid droplet formation.[10] Here we conduct a case study of $c_0a = 1$ and present the evolution of lipid droplet configurations, energy change, and contact area A_c in Fig. S5 (ESI†). In comparison with the case of $c_0 = 0$ (Fig. 3b), smaller $\bar{\gamma}$ is required for budding transition at $c_0a = 1$ (Fig. S5b, ESI†).

Extracting the critical values of $\bar{\gamma}$ in the curves of $\Delta E(\bar{\gamma})$ at given $\bar{\sigma}$ and c_0, we could determine the budding phase diagram with respect to normalized membrane tension $\bar{\sigma}$ and interfacial energy $\bar{\gamma}$ (Fig. 5). It is shown that the transition from the embedded state to the budding state is facilitated by $\bar{\gamma}$ and suppressed by $\bar{\sigma}$. In addition, $\bar{\gamma}$ for budding increases as the monolayer spontaneous curvature c_0 decreases from a positive value to a negative value. This is expected as the lipid monolayer of a positive c_0 prefers a bulge configuration to reduce the membrane bending energy. In short words, positive (negative) monolayer spontaneous curvature promotes (suppresses) the budding of an embedded lipid droplet. This is consistent with recent experimental studies that lipid molecules with negative intrinsic curvature such as diacylglycerol and phosphatidylethanolamine favor the embedded state for the lipid droplets, while lysolipids with positive intrinsic curvature facilitate the budding.[10] At each phase boundary, there is one position at which the tangent line passes through the origin $(\bar{\sigma}, \bar{\gamma}) = (0, 0)$ and the value of the corresponding slope is listed. For γ/σ smaller than that value at given c_0a, no matter how large a is, only the embedded state is achieved.

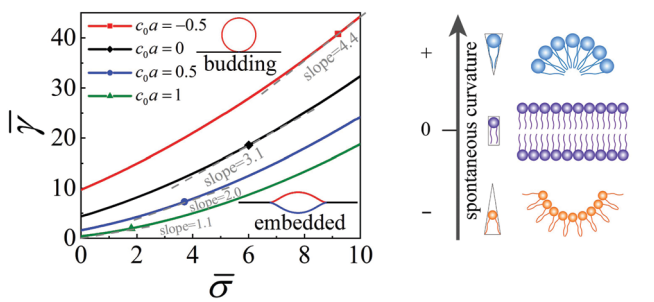

Fig. 5 Budding phase diagram with respect to $\bar{\sigma}$ and $\bar{\gamma}$ for two identical monolayers with $c_0a = -0.5$, 0, 0.5 and 1. Each dashed straight line passes through the origin and is tangent to the corresponding phase boundary at the marked place of slope $d\bar{\gamma}/d\bar{\sigma} = \gamma/\sigma$. Right panel: Illustration of monolayers of positive, zero, negative spontaneous curvatures.

3.2 A lipid droplet between two monolayers of different mechanical properties

In a more general case of a lipid droplet embedded between two chemically different lipid monolayers, the mechanical properties of two monolayers could be different. Consequently, the system in the embedded state could lose the vertical symmetry. In this subsection, we focus on this circumstance and consider the cases of such as bending rigidities ($\kappa_1 \neq \kappa_2$) and membrane tensions ($\sigma_1 \neq \sigma_2$) but with vanishing monolayer spontaneous curvature ($c_0 = 0$) without losing generality.

We first probe the membrane bulging at different bending rigidities. Fig. 6 shows the selected system morphologies at $\kappa_2 = 1.5\kappa_1 = 1.5\kappa$, $\sigma_1 = \sigma_2 = \sigma$, and $c_0 = 0$. It is shown that the

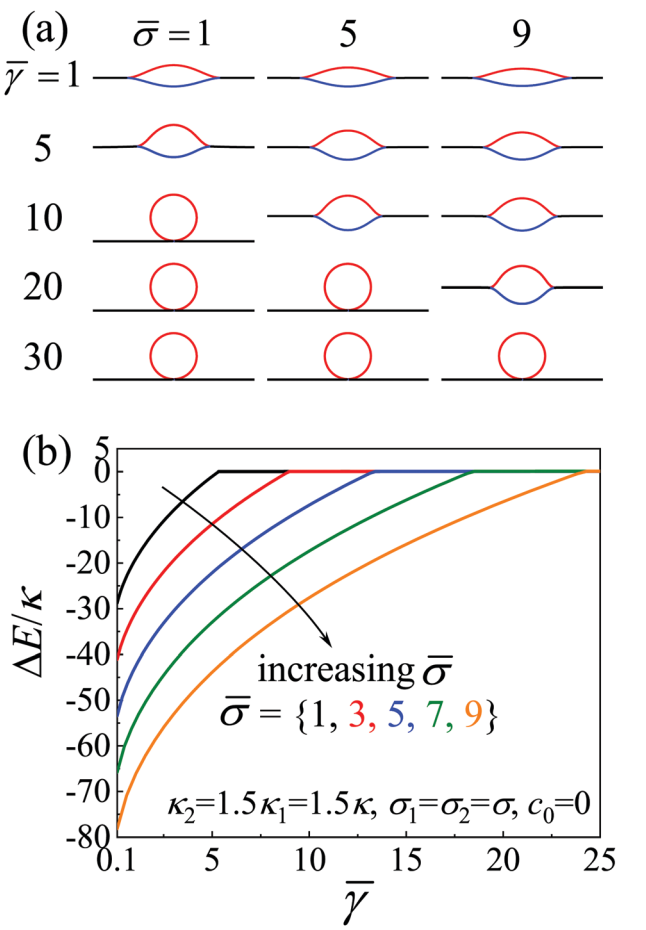

Fig. 6 Evolution of system configurations and energy for a lipid droplet between two monolayers of different mechanical properties of $\kappa_2 = 1.5\kappa_1 = 1.5\kappa$, $\sigma_1 = \sigma_2 = \sigma$, and $c_0 = 0$. (a) Selected system configurations at different sets of $(\bar{\sigma}, \bar{\gamma})$. (b) Profiles of the energy change ΔE.

embedded lipid droplet loses vertical symmetry before budding, exhibits more bulging toward the monolayer with a smaller bending rigidity to avoid a higher bending energy associated with the stiffer monolayer, and buds off from the softer monolayer eventually (Fig. 6a). The energy profiles $\Delta E(\bar{\gamma}) = E_{tot} - E_0$ as functions of $\bar{\gamma}$ at different $\bar{\sigma}$ are shown in Fig. 3b, where the energy E_0 of the ground state approximating the budding state is defined as $E_0 = 2\pi\kappa_1(2 - c_0a)^2 + 4\pi(\sigma + \gamma)a^2 + \pi(\kappa_1 + \kappa_2)c_0^2R_e^2/2$. In comparison with Fig. 3b ($\kappa_1 = \kappa_2 = \kappa$), the critical $\bar{\gamma}$ at the kink is smaller in Fig. 6b, which means that a smaller $\bar{\gamma}$ is required for the lipid droplet to bud off at $\kappa_2 > \kappa_1$.

Besides the case of unequal monolayer bending rigidities, we also investigate the case of $\sigma_1 \neq \sigma_2$ but $\kappa_1 = \kappa_2$ and $c_0 = 0$. In Fig. S6 (ESI†) ($\sigma_2 = 1.5\sigma_1 = 1.5\sigma$, $\kappa_2 = \kappa_1 = \kappa$, and $c_0 = 0$), the bulging before budding exhibits a similar vertical symmetry breaking as that observed in Fig. 6b. The lipid droplet buds toward the lipid monolayer of a smaller membrane tension to prevent a higher cost of the membrane tension energy. In addition, a larger membrane tension prefers a less biased budding at a given $\bar{\gamma}$, consistent with experimental observation that the artificial lipid droplet embedded in the bilayer of a giant unilamellar vesicle (GUV) upon a micropipette suction bulges into the GUV lumen.[7]

With the knowledge of the energy profiles $\Delta E(\bar{\gamma})$ as shown in Fig. 6 and Fig. S6 (ESI†), we extract the critical values of $\bar{\gamma}$ and determine the budding phase diagrams for a lipid droplet embedded between two lipid monolayers of different bending rigidities and membrane tensions (Fig. 7). As the ratio of κ_2/κ_1 or σ_2/σ_1 increases, the interfacial energy $\bar{\gamma}$ required for the budding transition decreases due to the less deformation of the lipid monolayer with a larger bending rigidity or tension. Note that $\bar{\sigma}$ in Fig. 7 is defined by the lower tension.

The budding phase diagrams in Fig. 5 and 7 indicate that the outward budding transition is facilitated by $\bar{\gamma}$ and suppressed by $\bar{\sigma}$, consistent with recent experimental studies in which artificial lipid droplets in giant unilamellar vesicles of different phospholipid composition show a clear budding transition and occurrence as the measured bilayer tension decreases below around 0.1 mN m^{-1}.[11]

The budding phase diagrams established in Fig. 5 and 7 enable us to estimate the critical lipid droplet size for budding transition. In Fig. 8 we extract the phase boundary at $c_0 = 0$ from Fig. 5 and plot the critical budding size as a function of γ for different σ at $\kappa = 10k_BT$ with the thermal energy $1k_BT = 4.1 \times 10^{-21}$ N m. Typical values of physical properties associated with ER membranes and lipid droplets are listed in Table 1.[11,26–31] At a given interfacial energy γ, the critical lipid droplet size a slightly decreases, agreeing with recent experiments showing that small lipid droplet sizes are favored for phospholipids exhibiting relatively low tension.[11] As γ decreases, a increases, relatively insensitive to σ. Recent experimental studies suggest that γ is around 1 mN m^{-1},[11] orders of magnitude larger than the ER bilayer membrane tension (around 0.013 mN m^{-1}).[27] Therefore, the critical size is expected to be around few tens of nanometers.[14,15] As shown in Fig. 8, the critical radius a is around 10 nm at $\gamma = 1$ mN m^{-1}. This predicted size as a lower bound of the lipid droplet size is significantly smaller than the experimentally observed size (ranging from 100 nm to around

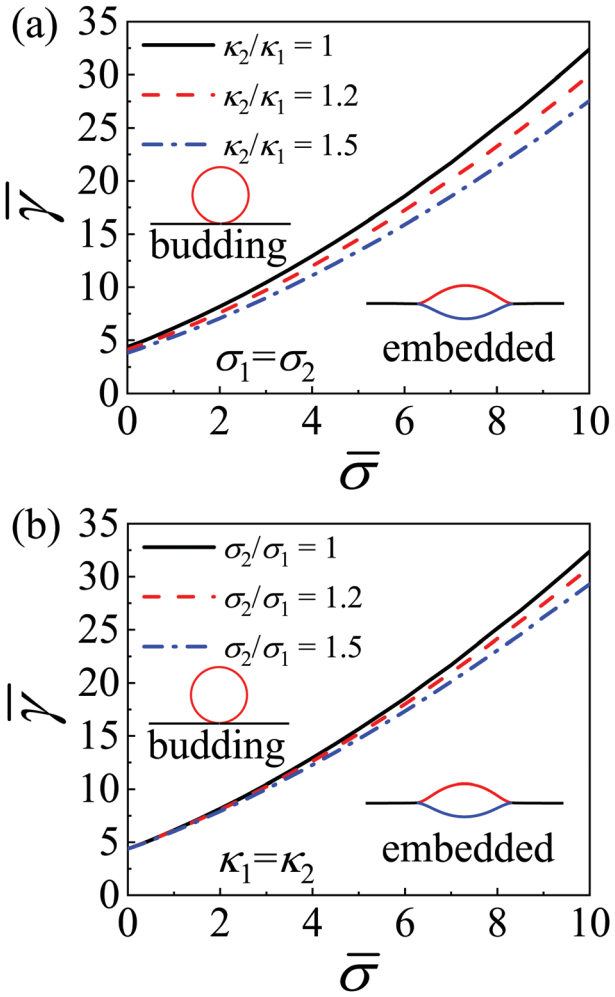

Fig. 7 Budding phase diagrams for different values of κ_2/κ_1 at $\sigma_1 = \sigma_2$ (a) and different values of σ_2/σ_1 at $\kappa_1 = \kappa_2$ (b) with $c_0 = 0$.

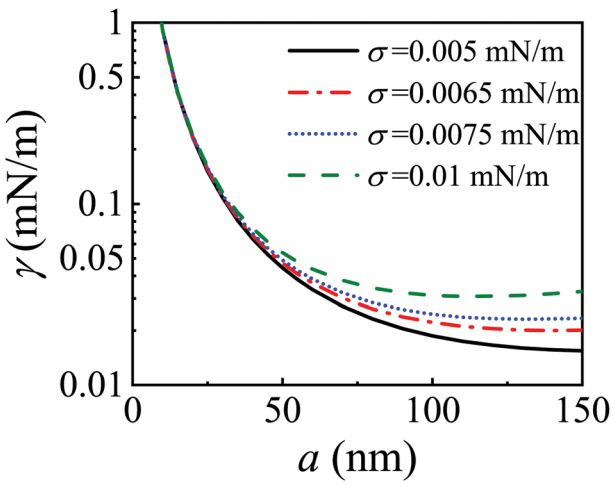

Fig. 8 Critical budding size with respect to different interfacial energy γ and monolayer tension σ at vanishing monolayer spontaneous curvature.

Table 1 Typical values of physical properties of lipid membranes and lipid droplets

Physical properties	Values	Ref.
Bending rigidity κ of lipid monolayer	$10k_BT$	26
ER bilayer tension	0.013 mN m^{-1}	27
Interfacial energy γ	1 mN m^{-1}	11
Spontaneous curvature	-0.05 nm^{-1} to 0.5 nm^{-1}	28
Lipid lens size	Tens of nanometers	3, 5 and 9
Size of lipid droplets	100 nm to 5 μm	29–31

5 μm in most cell types) of lipid droplets released from the ER[29–31] and in yeast mutants.[32] One possible reason for this discrepancy is that a freshly budded spherical lipid droplet with the critical size could further grow as more neutral lipids accumulate within the budded region.

In this work, the Helfrich membrane theory is adopted to investigate the lipid membrane deformation during bulging and budding of lipid droplets. Using this continuum theory, the lipid membranes are modelled as mathematical surfaces with zero thickness. In real situations, the overall thickness of cell membranes with consideration of the protrusion of membrane proteins could vary in a range of 4 nm to 10 nm, and a representative value of the thickness of simple lipid bilayers or cell membranes excluding protein protrusion is around 4 nm to 5 nm.[31] For endoplasmic reticulum membranes, the thickness is around 4 nm.[33] Recalling that the critical radius of curvature for the lipid droplet formation could be as small as 10 nm based on the present theoretical model (Fig. 8), readers might wonder whether the continuum membrane theory is still valid and applicable in cases with the membrane curvature radius comparable to the lipid bilayer thickness. By investigating the tensile force necessary for a stable membrane nanotube, a combination of molecular dynamics simulations and theoretical analysis indicates that the Helfrich membrane theory indeed remains valid and applicable for highly curved regimes with a radius of curvature down to a length scale comparable to the lipid bilayer thickness.[34] Therefore, the membranes can be modelled as mathematical surfaces here and the effect of membrane thickness on the present theoretical analysis is negligible.

As the measurement of the interfacial energy γ is not easy, especially in cellular conditions, eqn (14) of $\bar{\gamma} = (2a/R_j)^8$ may provide a valuable and relatively easy estimation on γ by measuring lipid droplet size a and the r-coordinate R_j of the layer junction.

A mechanical feature of the lipid droplet formation is that the embedded neutral lipids of a fixed volume can flow and deform easily or reorganize. Similar mechanical features are observed in drug loaded liposomes[35–37] and incorporation of nanoparticle clusters or decorated nanoparticles within lipid membranes.[38–41] For example, the microfluidic technique has be employed to fabricate multicompartment liposomes with residual oil droplets embedded in the lipid membranes.[36] For echogenic liposomes, microscale gas bubbles are formed in the lipid membranes.[35,37] In addition, experimental results show that the embedded hydrophobic nanoparticle cluster evolves from a lens-shaped to a spherical cap-shaped configuration, as more nanoparticles assemble and reorganize within the vesicle membrane.[38] For dendrimer-like soft nanoparticles[39] and amphiphilic polymer-decorated nanoparticles[40,41] undergoing cell interaction, they could become embedded within cell membranes and exhibit significant morphological transformation.

4 Conclusions

We have conducted a systematic theoretical study on the budging and budding of an embedded lipid droplet in a lipid bilayer membrane, taking into account the membrane asymmetry and spontaneous curvature. As the interfacial energy per unit area of contact between lipid droplet and monolayer interface increases, lipid droplets go through a discontinuous shape transition from a lens-like embedded shape to a budding state with a spherical bulge configuration. The shape transition is an energy driven process. The sharp decrease of interfacial contact area coordinating with a sharp increase of elastic energy yield a continuous total energy evolution while a kink emerges at the shape transition point. Analytical expression governing the lipid droplet morphology before budding transition has been obtained. Positive spontaneous curvature of monolayers can promote lipid droplets budding transition while negative spontaneous curvature inhibits this process. Moreover, the existence of monolayer bending rigidity asymmetry promotes budding transition and regulates budding direction toward the side with lower monolayer bending rigidity, and so as the asymmetry of monolayer tension. A rich variety of budding phase diagrams have been established for both symmetric and asymmetric situations, from which the lipid droplet budding size can be examined. Our results provide fundamental insights on the underlying physics of lipid droplet formation and are of interest to the studies of echogenic liposome stability and nanoparticle clustering within lipid membranes.

Conflicts of interest

There are no conflicts to declare.

Acknowledgements

This work was supported by the National Natural Science Foundation of China (Grant No. 11872005 and 12022207). Computation resources supported by the High-performance Computing Platform of Peking University are acknowledged.

References

1 A. R. Thiam, R. V. Farese Jr and T. C. Walther, *Nat. Rev. Mol. Cell Biol.*, 2013, **14**, 775–786.
2 F. Wilfling, J. T. Haas, T. C. Walther and R. V. Farese Jr, *Curr. Opin. Cell Biol.*, 2014, **29**, 39–45.
3 J. A. Olzmann and P. Carvalho, *Nat. Rev. Mol. Cell Biol.*, 2019, **20**, 137–155.
4 N. L. Gluchowski, M. Becuwe, T. C. Walther and R. V. Farese Jr, *Nat. Rev. Gastroenterol. Hepatol.*, 2017, **14**, 343–355.
5 A. R. Thiam and L. Forêt, *Biochim. Biophys. Acta*, 2016, **1861**, 715–722.
6 K. D. Chapman, M. Aziz, J. M. Dyer and R. T. Mullen, *Biochem. J.*, 2019, **476**, 1929–1942.
7 A. Chorlay and A. R. Thiam, *Biophys. J.*, 2018, **114**, 631–640.
8 A. Chorlay, *et al.*, *Dev. Cell*, 2019, **50**, 25–42.
9 V. Choudhary, N. Ojha, A. Golden and W. A. Prinz, *J. Cell Biol.*, 2015, **211**, 261–271.
10 V. Choudhary, G. Golani, A. S. Joshi, S. Cottier, R. Schneiter, W. A. Prinz and M. M. Kozlov, *Curr. Biol.*, 2018, **28**, 915–926.
11 K. B. M'barek, D. Ajjaji, A. Chorlay, S. Vanni, L. Forêt and A. R. Thiam, *Dev. Cell*, 2017, **41**, 591–604.
12 V. Zoni, V. Nieto, L. J. Endter, H. J. Risselada, L. Monticelli and S. Vanni, *Front. Mol. Biosci.*, 2019, **6**, 124.
13 V. Zoni, R. Khaddaj, P. Campomanes, A. R. Thiam, R. Schneiter and S. Vanni, *BioRxiv*, 2020, DOI: 10.1101/777466.
14 J. Zanghellini, F. Wodlei and H. H. von Grünberg, *J. Theor. Biol.*, 2010, **264**, 952–961.
15 F. Deslandes, A. R. Thiam and L. Forêt, *Biophys. J.*, 2017, **113**, 15–18.
16 W. Helfrich, *Z. Naturforsch., C: Biochem., Biophys., Biol., Virol.*, 1973, **28**, 693–703.
17 T. C. Walther and R. V. Farese Jr, *Biochim. Biophys. Acta*, 2009, **1791**, 459–466.
18 Z. Wu and X. Yi, *J. Mech. Phys. Solids*, 2020, **137**, 103867.
19 J. B. Fournier, *Soft Matter*, 2007, **3**, 883–888.
20 X. Tang, J. Wang and X. Yi, *J. Appl. Mech.*, 2019, **86**, 121002.
21 B. Fourcade, L. Miao, M. Rao, M. Wortis and P. K. P. Zia, *Phys. Rev. E: Stat., Nonlinear, Soft Matter Phys.*, 1994, **49**, 5276–5286.
22 Z.-l. Li, H.-m. Ding and Y.-q. Ma, *Soft Matter*, 2013, **9**, 1281–1286.
23 T. Yue, H. Zhou, H. Sun, S. Li, X. Zhang, D. Cao, X. Yi and B. Yan, *Nanoscale*, 2019, **11**, 6602–6609.
24 L. Foret, *Eur. Phys. J. E: Soft Matter Biol. Phys.*, 2014, **37**, 42.
25 J. Zimmerberg and M. M. Kozlov, *Nat. Rev. Mol. Cell Biol.*, 2006, **7**, 9–19.
26 P. Méléard, C. Gerbeaud, T. Pott, L. Fernandez-Puente, I. Bivas, M. D. Mitov, J. Dufourcq and P. Bothorel, *Biophys. J.*, 1997, **72**, 2616–2629.
27 A. Upadhyaya and M. P. Sheetz, *Biophys. J.*, 2004, **86**, 2923–2928.
28 N. Fuller and R. P. Rand, *Biophys. J.*, 2001, **81**, 243–254.
29 R. Uzbekov and P. Roingeard, *BMC Res. Notes*, 2013, **6**, 386.
30 S. Mishra, R. Khaddaj, S. Cottier, V. Stradalova, C. Jacob and R. Schneiter, *J. Cell Sci.*, 2016, **129**, 3803–3815.
31 B. Alberts, A. D. Johnson, J. Lewis, D. Morgan, M. Raff, K. Roberts and P. Walter, *Molecular Biology of the Cell*, Garland Science, Taylor & Francis Group, New York, 6th edn, 2015.
32 T. Czabany, A. Wagner, D. Zweytick, K. Lohner, E. Leitner, E. Ingolic and G. Daum, *J. Biol. Chem.*, 2008, **283**, 17065–17074.
33 K. Mitra, I. Ubarretxena-Belandia, T. Taguchi, G. Warren and D. M. Engelman, *Proc. Natl. Acad. Sci. U. S. A.*, 2004, **101**, 4083–4088.
34 V. A. Harmandaris and M. Deserno, *J. Chem. Phys.*, 2006, **125**, 204905.
35 S. M. Fix, M. A. Borden and P. A. Dayton, *J. Controlled Release*, 2015, **209**, 139–149.
36 N. N. Deng, M. Yelleswarapu and W. T. S. Huck, *J. Am. Chem. Soc.*, 2016, **138**, 7584–7591.
37 N. Güvener, L. Appold, F. de Lorenzi, S. K. Golombek, L. Y. Rizzo, T. Lammers and F. Kiessling, *Methods*, 2017, **130**, 4–13.
38 C. Bonnaud, C. A. Monnier, D. Demurtas, C. Jud, D. Vanhecke, X. Montet, R. Hovius, M. Lattuada, B. Rothen-Rutishauser and A. Petri-Fink, *ACS Nano*, 2014, **8**, 3451–3460.
39 R. Guo, J. Mao and L.-T. Yan, *ACS Nano*, 2013, **7**, 10646–10653.
40 Z. Shen, H. Ye, M. Kröger and Y. Li, *Nanoscale*, 2018, **10**, 4545–4560.
41 Y. Liu, S. Li, X. Liu, H. Sun, T. Yue, X. Zhang, B. Yan and D. Cao, *ACS Appl. Mater. Interfaces*, 2019, **11**, 23822–23831.

Supplementary Information for
"Bulging and budding of lipid droplets from symmetric and asymmetric membranes: Competition between membrane elastic energy and interfacial energy"

Meng Wang and Xin Yi
Department of Mechanics and Engineering Science, College of Engineering,
Peking University, Beijing 100871, China

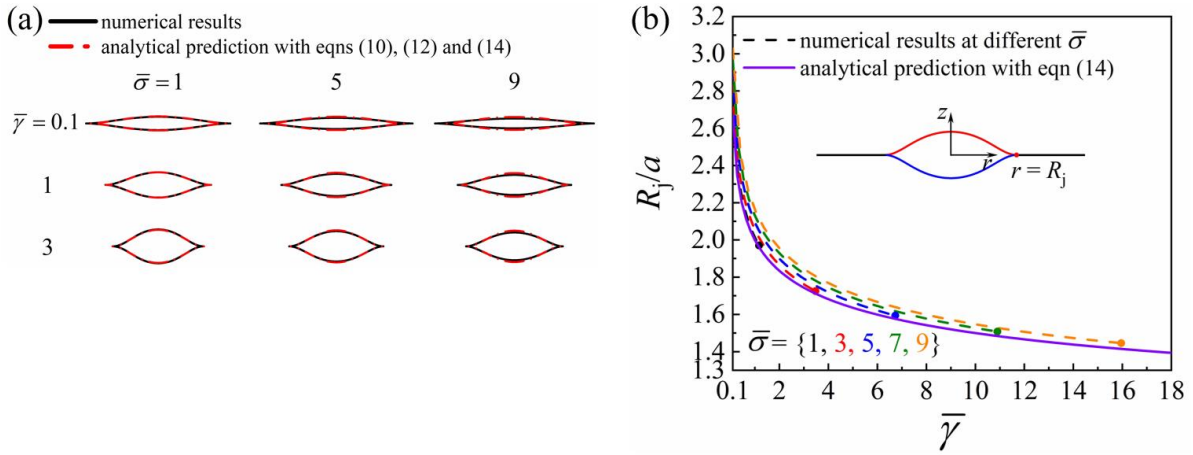

Fig. S1 Comparison between our numerical results using optimization and analytical prediction at $c_0=1/a$. (a) Selected shapes of contact regions, and (b) r-coordinate R_j of the triple junction.

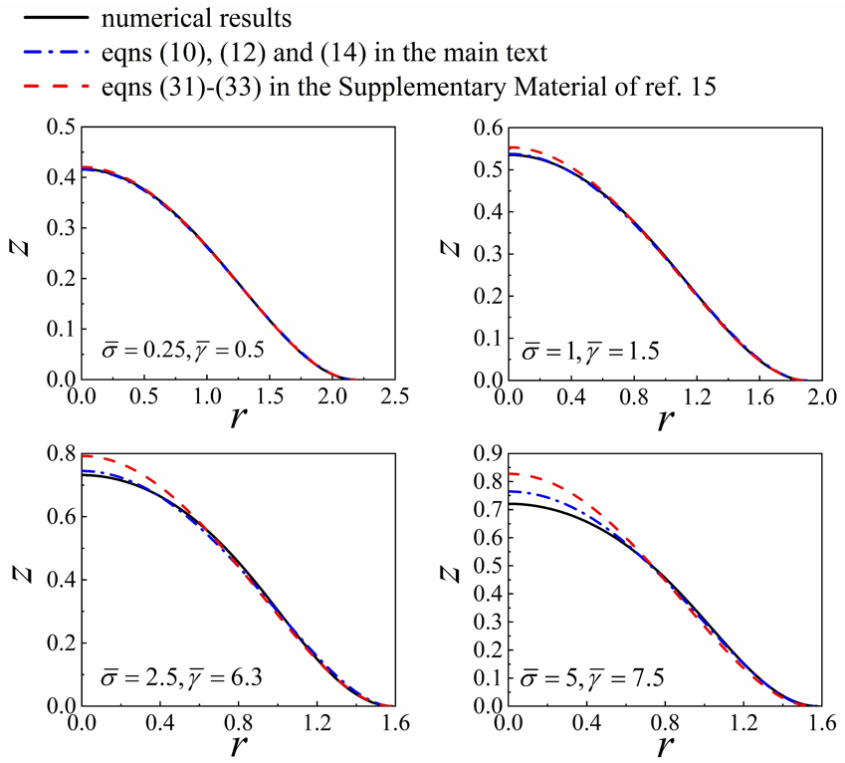

Fig. S2 Bulging profiles in the cases of two identical monolayers at $c_0=0$. Comparing the present fully nonlinear numerical results (black lines) and small deformation based analytical solutions (blue dash-dotted lines) with another small deformation based analytical predictions (red dashed lines) in the Supplementary Material of ref. 15. The small deformation assumption adopted in ref. 15 has been used in characterizing the membrane geometry as well as the membrane forces and their balance but in an inconsistent way.

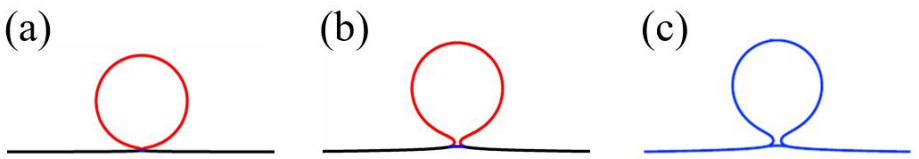

Fig. S3 System configurations in the budding state for two identical monolayers at $\bar{\sigma}=0$, $\bar{\gamma}=3.4$, and c_0=0. Numerical results based on the energy optimization with dense meshing (a) and loose meshing (b) in the vicinity of the highly curved neck regions. (c) The system configuration from Supplementary Material of ref. 15. The configuration (a) with dense meshing has a slightly lower energy of E_{tot}/κ=46.495 in comparison with E_{tot}/κ=46.636 for the configuration (b) mimicking reported configuration (c). It is indicated that the system configuration with a relatively large neck reported in ref. 15 might have a higher system energy than that with an extremely narrow neck, and the discrepancy suggests that a more appropriate initial guess is required for the shooting method in ref. 15.

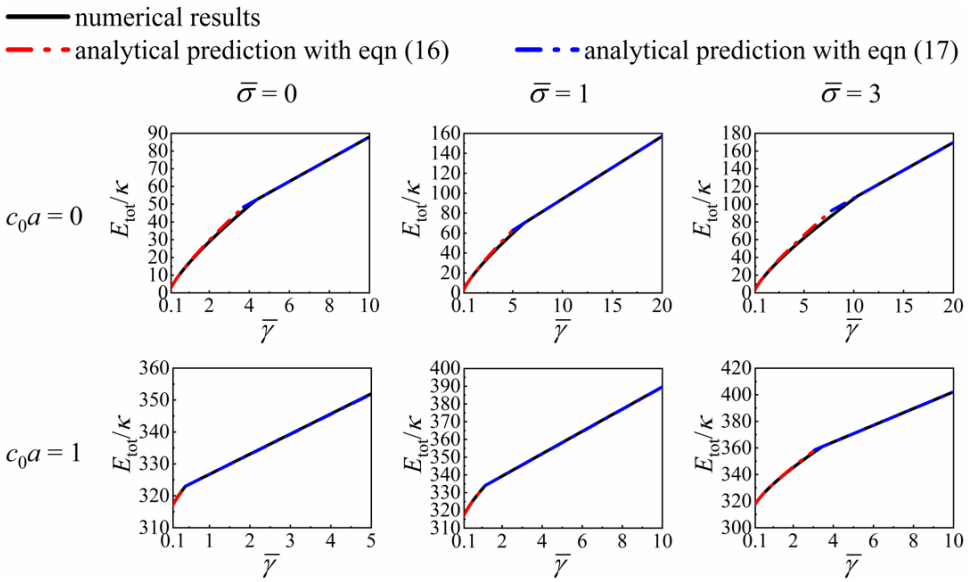

Fig. S4 Comparison of the total system energy E_{tot} between fully nonlinear numerical results and theoretical predictions given by eqn (16) and eqn (17) in the main text. The kinks in curves represent the critical values of $\bar{\gamma}$ associated with the budding transition.

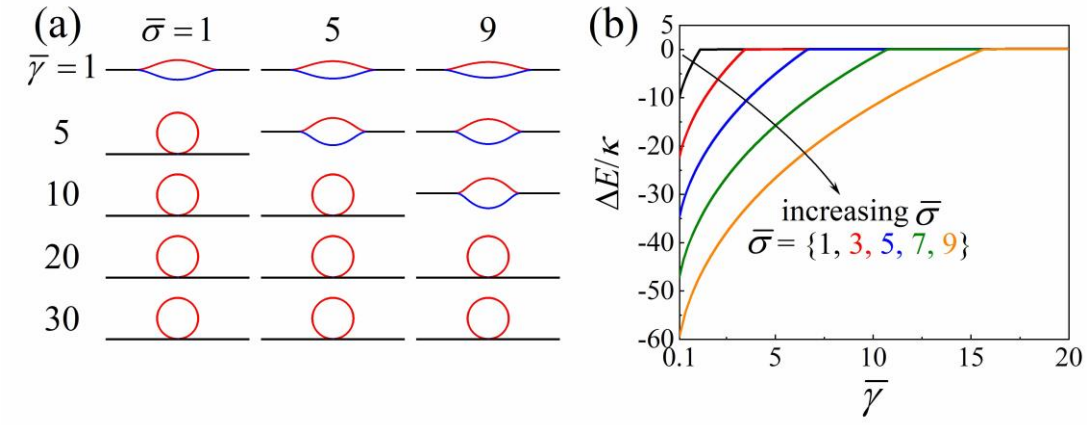

Fig. S5 Evolution of lipid droplet configurations and total energy change for the case of two identical monolayers with c_0=1/a. (a) Selected lipid droplet configurations at different sets of $(\bar{\sigma},\bar{\gamma})$. (b) Energy change ΔE as a function of $\bar{\gamma}$.

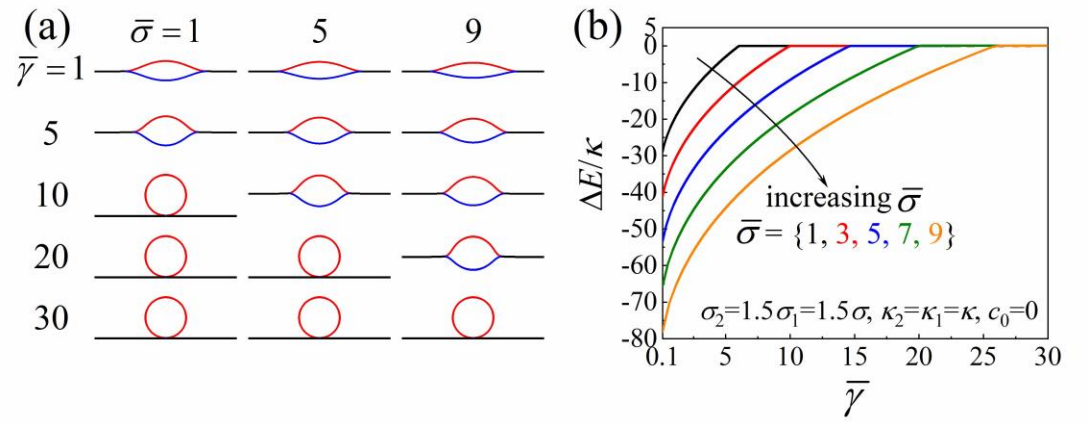

Fig. S6 Evolution of the system configurations and total energy change for a lipid droplet between two monolayers of different mechanical properties of σ_2=1.5σ_1=1.5σ, κ_2=κ_1=κ, and c_0=0. (a) Selected system configurations at different sets of $(\bar{\sigma},\bar{\gamma})$. (b) Profiles of the energy change ΔE.